ISSN 1990-7931, Russian Journal of Physical Chemistry B, 2014, Vol. 8, No. 2, pp. 158–164. © Pleiades Publishing, Ltd., 2014.
Original Russian Text © A.A. Borisov, A.S. Koval', A.E. Mailkov, V.A. Smetanyuk, S.M. Frolov, 2014, published in Khimicheskaya Fizika, 2014, Vol. 33, No. 3, pp. 27–34.

COMBUSTION, EXPLOSION, AND SHOCK WAVES

Transient Modes of Propagation of the Shock Wave–Reaction Zone Complex in Methane–Air Mixtures

A. A. Borisov[a], A. S. Koval'[a], A. E. Mailkov[a], V. A. Smetanyuk[a], and S. M. Frolov[a, b, *]

[a] *Center for Pulse-Detonation Combustion, Semenov Institute of Chemical Physics, Russian Academy of Sciences, Moscow, Russia*

[b] *National Research Nuclear University "MEPhI", Moscow, Russia*

**e-mail: smfrol@chph.ras.ru*

Received June 3, 2013

Abstract—The dynamics of the combustion of stoichiometric methane–air mixtures during the passage from a larger-diameter to a smaller-diameter tube is experimentally studied. The combined effect of increases in the velocity and duration of the gas flow and in the degree of its turbulization due to a decrease in the cross sectional area of the tube and installation in it of turbulizing obstacles considerably enhance the probability of onset of combustion mode with the formation of strong shock waves. Combustion waves led by a shock wave that ignites the mixture at obstacles and propagates at a velocity of up to 1400 m/s within a distance of ~14 tube diameters are produced.

Keywords: methane–air mixtures, combustion, shock waves

DOI: 10.1134/S1990793114020043

INTRODUCTION

Methane, the main component of natural gas, is a combustible gas most commonly used in practice. Methane–air mixtures may be formed in a variety of conditions, in both confined and unconfined spaces. The explosibility of such mixtures has been investigated for several hundred years.

Although detonation in methane–air mixtures is very difficult to initiate due to the low reactivity of methane in reactions with air oxygen, a detonative explosion is traditionally considered the most dangerous and destructive. At present, it is generally accepted that the smallest diameter of a smooth tube in which the detonation of a methane–air mixture can be initiated under normal conditions (for example, by a detonation wave propagating from an oxygen-based mixture, an active charge explosion, or by the gasdynamic focusing of a relatively weak shock wave) is 80–100 mm (see, e.g., [1–3]), although there is evidence [4] on the possibility of direct initiation of detonation (likely overdriven detonation) in a tube of diameter 50 mm. The critical energy of direct detonation initiation in methane–air mixtures in tubes reaches 50–70 g of HE [2, 5] or 9–10 MJ/m^2 [4, 6].

Today we can only assume that the detonability limits of methane–air mixtures in tubes for a strong initiation and deflagration-to-detonation transition (DDT) are close to each other. The fact is that the published data on DDT in tubes with methane–air mixtures are contradictory. For example, according to the estimates made in [2, 7], the predetonation distance for a stoichiometric methane–air mixture in a smooth tube should reach 50–125 tube diameters; however, today there is neither experimental evidence supporting these estimates, nor facts about the very possibility of DDT in smooth tubes. The availability of regular obstacles inside the tube shortens the predetonation length to 20–30 tube diameters [8–17]. However, according to [9, 10], under normal conditions, the critical tube diameter reduces to 50 mm [9], or even to 36 mm [10], whereas according to [11, 12], it remains the same as for direct detonation initiation (100 mm [11], or ~94 mm [12]), while according to [13], it increases (the authors of [13] reported that, in a 121-mm-diameter tube with regular annular turbulizing obstacles, DDT in a stoichiometric methane–air mixture is possible only at initial pressures above 2 atm). In all these cases, it is assumed that detonation wave formed as a result of DDT can propagate in a self-sustaining manner in a smooth section attached to the tube's section with turbulizing obstacles.

Note that, in contrast to [9, 10, 13], where regular annular turbulizing obstacles or a Shchelkin spiral were used, in [11], special patented turbulizing obstacles were employed, whereas in [12], specially profiled turbulizing obstacles were used to ensure an optimal harmonization of the rates of flame acceleration and strengthening of the shock wave generated by the flame, so as to provide conditions for rapid DDT (according to the terminology of [18]).

Along with detonation, there are other explosive modes. Of greatest interest from the point of view of

explosion safety are modes of combustion of methane–air mixtures with the formation of intense pressure waves capable of producing significant destruction. Such modes are transient between flame propagation at apparent velocities of several tens of meters per second and normal detonation propagating at velocities of 1600–1800 m/s. The transient combustion modes include so-called galloping detonation [1], for which detonation regions alternate with regions where the shock wave and the flame front are separated, as well as nonideal detonation in rough tubes and tubes with regular obstacles [19–22], for which the flame and shock wave are sufficiently stably connected with each other only at the periphery of the tube due to the self-ignition of the mixture in areas of reflection of the shock wave from roughness elements or obstacles. In the literature, all these modes are referred to by one term: fast deflagration combustion.

When studying such destructive combustion modes, it is important not only to assess the possibility of their occurrence, but also to identify the conditions under which they arise within a short distances from the ignition source. The latter is important for assessing the risks of accidents and for designing the equipment for explosion hazard productions. In addition, it is important for the practical use of transient combustion regimes in various technological devices [23], for example, in new-type pulse-detonation burners, which provide a combined effect on objects blown on with combustion products: shock-wave (mechanical) and thermal [12, 16].

The aim of the present experimental work is to determine the conditions under which rapid combustion modes with intense shock waves, similar to the detonation mode, can arise as a result of mixture ignition with a source that does not generate initial shock waves. For this purpose, we specially selected such geometric parameters of the tube that are not best for DDT, namely: (1) the tube diameter was 70 mm, which provided [1] a steady propagation of detonation in a 17-m-long smooth tube only in stoichiometric methane mixture, and even so with noticeable wave velocity fluctuations; (2) the length of the section over which the development of the process was recorded did not exceed 2.5 m.

EXPERIMENTAL FACILITY

The rapid development of turbulence in the gas stream ahead of the flame is known to be one of the major factors that accelerate flame propagation and, hence, the formation of an intense pressure wave. There are two ways of intensification of turbulence in the flow: to place turbulizing obstacles [8] and to increase in the gas flow velocity [12, 15, 16]. While the first method is widely used in studies of DDT [9–22], the second one has received less attention. In most practical situations, the gas mixture is initially at rest, so that a high flow velocity can arise only in the course of the combustion process itself due to the expansion

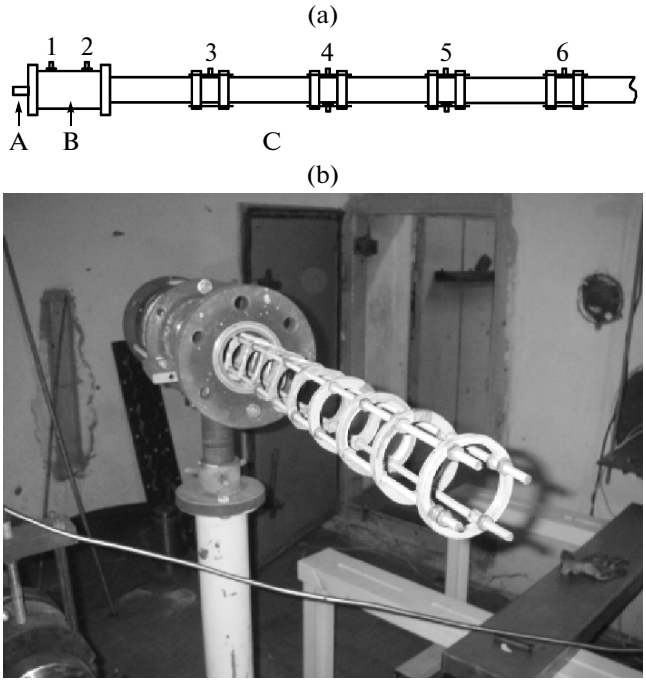

Fig. 1. (a) Schematic diagram of the experimental setup and (b) photograph of turbulizing obstacles.

of the reaction products. In reality, combustion can arise in a large volume and then move on to other volumes through channels where the flow ahead of the flame accelerates dramatically.

In the present work, we used both approaches to accelerating the combustion process: by creating an initial turbulent gas flow and by making the flame become turbulized on obstacles. Figure 1a shows a schematic diagram of the experimental facility. It consists of three interconnected sections: a precombustion chamber (A), booster (B) and test section (C) with turbulizing obstacles. The precombustion chamber is intended for reliable mixture ignition in the booster; the booster serves to create an initial turbulent gas flow in the test section; the turbulizing obstacles in the test section additionally turbulize the flame and create hot spots as shock waves are reflected.

In most experiments, the precombustion chamber was a tube 51 mm in inner diameter and 180 mm in length (its volume was 0.37 L). Near the closed end of the precombustion chamber, a spark ignition source was placed, whereas its open end communicated with the booster through a flow-restricting washer with a circular central hole of diameter 16 mm. In what follows, these experiments will be referred to as experiments without activation. In some experiments, the precombustion chamber was a tube with internal diameter of 12.7 mm and a length of 800 mm (with a volume of 0.1 L) with two closed ends. One end accommodated an ignition source in the form of an electrically fused wire, whereas the other had six 3-mm-diameter radial holes evenly spaced over the

perimeter of the tube cross section. The portion of the tube with holes was slightly deepened into the booster via an adapter. Experiments with such a precombustion chamber will be referred to as experiments with activation.

In the experiments without activating, the precombustion chamber, booster and test section were filled with a stoichiometric methane–air mixture. The experiments with activation were performed to investigate how the ignition energy and power influence the development of the explosion process: the precombustion chamber was filled with a stoichiometric methane–oxygen mixture; the amount of mixture introduced, determined from the pressure drop in 1-L bottle, did not exceed 0.1 L. In all cases, the methane–air mixture in the booster was ignited by one or more turbulent jets of combustion products outflowing from the precombustion chamber through the flow-restricting washer or the radial holes.

The booster was a straight tube 130 mm in diameter and 280 mm in length, one end of which communicated with the precombustion chamber, while the other, with the test section. To speed up the combustion of the mixture, a partition with twelve 14-mm-diameter holes evenly spaced along its perimeter was placed in the booster. In some experiments, the booster was additionally equipped with a second partition (downstream of the first) with eight holes of diameter 14 mm.

The test section was a straight tube with a diameter of 70 mm and a length of 2.5 m, one end of which communicated with the booster, whereas the other was open to atmosphere. The open end of the test section enabled to introduce in it a 0.5- to 1.5-m-long assembly of identical turbulizing obstacles (Fig. 1b). A single turbulizing obstacle was an orifice plate with external and internal diameters of 70 and 50 mm, respectively, and a thickness of 4 mm. The flow blockage ratio of such an orifice plate equals 0.49. In some experiments, a ring aperture with a blockage ratio of 0.67 was placed between the buster and the test section.

Stoichiometric methane–air mixture was prepared manometrically in a large-volume (30 L) mixer equipped with a fan for forced mixing, at a pressure up to 3 atm. In experiments without activation, the mixture was introduced through the precombustion chamber, with the amount of mixture flushed through the facility before ignition being not less than the 8- to 9-fold volume of the facility. In experiments with activation, a 0.1-L methane–oxygen mixture portion was injected into the precombustion chamber immediately before ignition.

The data-acquisition system included two low-frequency and four high-frequency pressure sensors and two photodiodes. Low-frequency pressure sensors 1 and 2 (Fig. 1a) were installed in the booster, whereas high-frequency sensors 3–6, in the test section. Photodiodes L1 and L2 were mounted in the same sections as the high-pressure sensors. The signals from the pressure sensors and photodiodes were fed into a personal computer via an analog-to-digital converter. The pressure sensor signals were used to measure the velocity of propagation of arising pressure waves (the maximum relative error was estimated as 5%, with allowance for the possible blurring of the front). The pressure sensors were not pressure-calibrated, so the analysis was based only on the measured velocities of the wave fronts. The signals from the photodiodes made it possible to determine the position of the light emission front relative to the wave front, as well as the average speed of propagation and the characteristic width of the emission front (relative error in determining the front velocity was 10%, taking into account the field of view of the photodiode).

The energy and power of the ignition pulse in the precombustion chamber (with and without ignition activation), the number of perforated partitions in the booster (experiments with one and two partitions), the configuration of the test section (experiments with and without the turbulizing obstacles), and the configuration of the joint between the booster and test section (with and without the ring aperture) were varied in the experiments.

EXPERIMENTAL RESULTS AND DISCUSSION

For convenience of presenting the experimental results, Table 1 lists the conditions of some representative experiments (I–VI), whereas Table 2, information on the location of the pressure sensors and photodiodes in these experiments (the distance to the sensor/photodiode was measured from the inner wall of the booster from the side of the precombustion chamber).

The purpose of experiments I and II was to determine the structure of the pressure waves in the smooth portion of the test section of the tube, i.e., in the absence of turbulizing obstacles. In experiment I (Fig. 2a), only stoichiometric methane–oxygen mixture was used (0.1 L), so that, before ignition, the fuel mixture filled only the precombustion chamber, while the booster and the test section were filled with air. In experiment II (Fig. 2b), the entire setup was filled with a methane–air mixture, while the process of ignition was activated by additionally introducing 0.1 L of stoichiometric methane–oxygen mixture into the precombustion chamber.

The signals from pressure sensor 2 in the booster in experiments I and II (signal 2 in Fig. 2) show a fairly fast (within 200–300 μs) pressure rise to a maximum at the initial stage of the process, which corresponds to the combustion of the methane–oxygen mixture in the precombustion chamber. The initial pressure peak is followed by a staged slow (on average) secondary pressure rise for approximately 1 ms due to the afterburning of unreacted methane–oxygen mixture, displaced from precombustion chamber into booster and mixed there with the surrounding gas. Here and below, the time origin was selected for each experiment individually, so data analysis must deal only with time intervals.

Table 1. Conditions of representative experiments

Run no.	Filling with methane–air mixture	Activation of ignition with a methane–oxygen mixture	Number of partitions in the booster	Presence/absence of the ring aperture between the booster and test section	Presence/absence of turbulizing obstacles in the test section
I	No	Yes	One	No	No
II	Full	Yes	One	No	No
III	No	Yes	One	No	Yes
IV	Full	Yes	One	No	Yes
V	Full	No	Two	No	Yes
VI	Full	No	Two	Yes	Yes

Table 2. Placement of pressure sensors 1–6 and photodiodes L1 and L2 (in mm)

Run no.	1	2	3	4	5	6	L1	L2
I	20	260	613	945	985	1317	945	1317
II	20	260	613	945	985	1317	945	1317
III	20	260	613	945	1277	1617	945	1277
IV	20	260	613	945	1277	1617	945	1277
V	20	613	945	1277	1617	1982	1277	1617
VI	20	260	613	945	1277	1617	945	1277

The structure of pressure waves propagating in the test section of the tube (pressure signals 3–6 in Fig. 2) largely corresponds to the profile of the signal recorded by sensor 2 in the booster. It features a primary shock wave and a number of secondary pressure waves, producing a stepwise, but slower (average) pressure rise.

A comparison of Figs. 2a and 2b shows that the primary shock wave is formed due to a rapid burnout of the methane–oxygen mixture in the precombustion chamber. In experiment I (Fig. 2a), the velocity of the primary shock wave in the test section is essentially constant, 400–450 m/s, whereas in experiment II (Fig. 2b), it increases from 400–450 m/s at the beginning of the test section to 600–650 m/s at its end. Since a series of secondary pressure waves is recorded in the test section in both experiment I (Fig. 2a), and experiment II (Fig. 2b), their formation is associated with the outflow of the gas from the precombustion chamber into the booster and then into the test section.

In experiment I (Fig. 2a), the apparent velocity of the first (in the series) of the secondary pressure waves propagating in the cocurrent gas flow behind the pri-

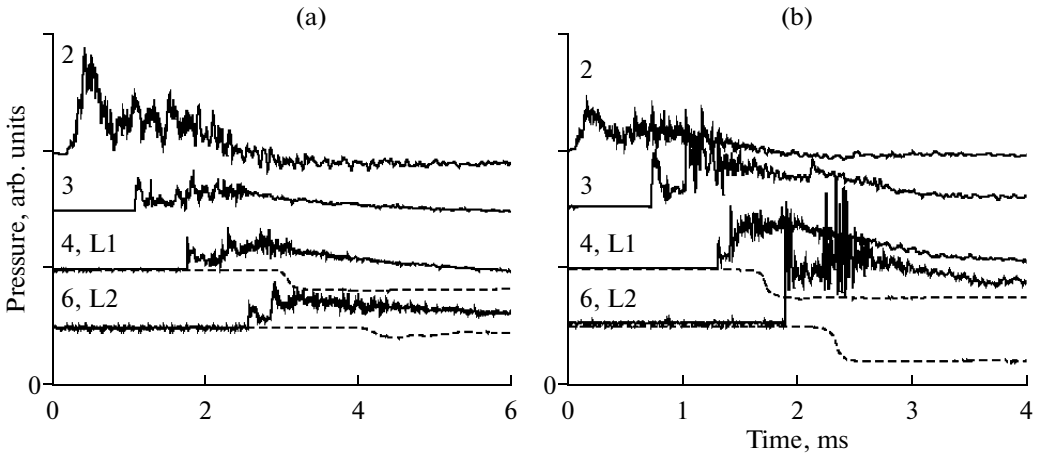

Fig. 2. Pressure profiles recorded by sensors 2–4 and 6 (solid curves) and luminescence intensity profiles recorded by photodiodes L1 and L2 (dashed curves) in experiments (a) I and (b) II.

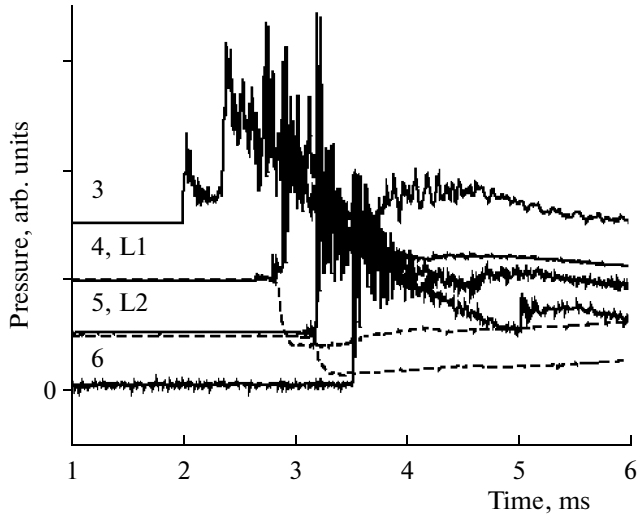

Fig. 3. Pressure profiles recorded by sensors 3–6 (solid curves) and luminescence intensity profiles recorded by photodiodes L1 and L2 (dashed curves) in experiment IV.

mary shock wave is about 550–600 m/s. Pressure signals 3, 4, and 6 (Fig. 2a) show that behind the first of the secondary waves there is another flat pressure peak, corresponding to the second of the secondary pressure waves. It is interesting that, at the end of the test section (pressure signal 6 in Fig. 2a), the first secondary wave is transformed into a relatively weak shock wave with a sharp front.

In experiment II (Fig. 2b), combustion in the booster and test section causes a significant strengthening of the secondary pressure waves. For example, the first of the secondary pressure waves transforms into a shock wave with a steep front early in the test section (pressure signal 3 in Fig. 2b), merging with the primary shock wave at the end of this section (curve 6 in Fig. 2b). Pressure signal 4 (Fig. 2b) recorded behind the first of the secondary shock waves clearly shows two smooth pressure peaks, belonging to the second and third secondary waves. In signal 6 (Fig. 2b), these waves appear as secondary shock waves with a sharp front.

An analysis of the photodiode signals (dashed lines in Fig. 2) shows that the apparent average velocity of the luminescent combustion products between sensors L1 and L2 in experiment I was ~300 m/s, whereas in experiment II, 550–600 m/s. Note that, in experiment II, the position of the luminescence front nearly coincides with the position of the pressure peak in one of the secondary waves (compare signal curves 4 and L1 in Fig. 2b). In this connection, we would like to point out that the local self-ignition of the methane mixture in such conditions is unlikely, so that the indicated position of the luminescence front is likely associated with the position of the flame front.

The purpose of experiments III and IV was to determine the structure of the pressure waves in the obstructed section, i.e., with the insert of turbulizing obstacles. In both experiments, the first turbulizing obstacle was located at a distance of 610 mm from the beginning of the booster, and the portion of the test section from the booster to the first turbulizing obstacle was smooth. All other conditions in experiment III were the same as in experiment I, whereas in experiment IV as in experiment II. Within this smooth portion of the test section, the flow patterns in experiments I–IV were very similar, both qualitatively and quantitatively. For example, Fig. 3 shows the pressure waveform (recorded by sensors 3–6), emission signals (recorded by photodiodes L1 and L2) in experiment IV. A comparison of Fig. 3 with Fig. 2b shows that the signal from pressure sensor 3 in experiments I and IV are very similar. In both experiments, the mean velocity of the primary shock wave within this portion of the test section was ~450–500 m/s.

At the same time, series of experiments I–II and III–IV show different flow patterns within the portion of the test section with turbulizing obstacles. While for experiments I and III, this difference consists only in a weakening of the primary shock waves in experiment III due to momentum loss [24], experiments II and IV feature a significant qualitative difference. Indeed, the signal from sensor 4 (Fig. 3) located inside the assembly of turbulizing obstacles shows a sharp increase of pressure in the primary shock wave caused by the merger with an intense secondary wave, with the amplitude of the formed shock wave being approximately an order of magnitude greater than the amplitude of the primary shock wave within the smooth portion of the test section. Such a wave can arise only when a significant amount of mixture locally explodes. The cause of the explosion can be either the rapid combustion of a strongly turbulized mixture near obstacles after the arrival of the flame or the self-ignition of local mixture volumes during multiple reflections of the shock wave from obstacles. In our opinion, the fact that the front of the shock wave (pressure signals 4 and 5 in Fig. 3) practically coincides with the luminescence front (signals L1 and L2) provides more evidence in favor of the second mechanism: the local self-ignition of the mixture at multiple reflections of the shock wave from obstacles. In other words, the shock wave–reaction zone complex propagates here by the mechanism of detonation in rough tubes [19–22]. Analysis of pressure waveforms in Fig. 3 shows that in the region o turbulizing obtastacles this complex accelerates to ~1000 m/s.

In experiments I–IV, the primary shock wave was initiated by using a small amount of methane–oxygen mixture supplied to the precombustion chamber. The question arises whether explosive processes such as that shown in Fig. 3 are possible in the ignition of a stoichiometric methane–air without activation. To answer this question, consider the results of experiment V (Table 1).

In experiment V, the setup was purged before ignition with a stoichiometric methane–air mixture, but in contrast to experiments II and IV, we used a 0.37 L precombustion chamber and no methane–oxygen

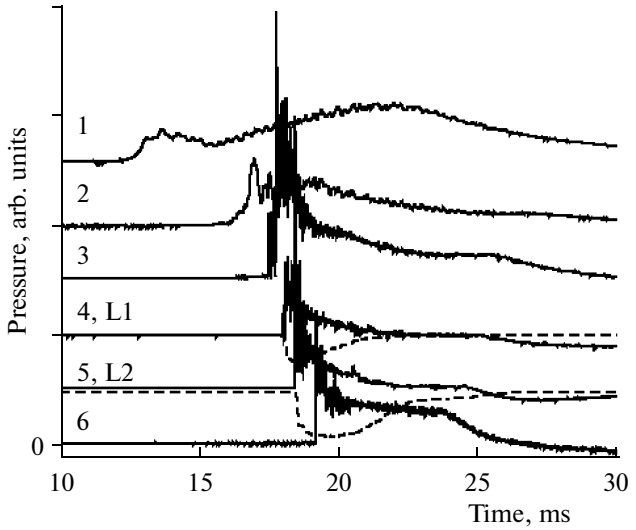

Fig. 4. Pressure profiles recorded by sensors 1–6 (solid curves) and luminescence intensity profiles recorded by photodiodes L1 and L2 (dashed curves) in experiment V.

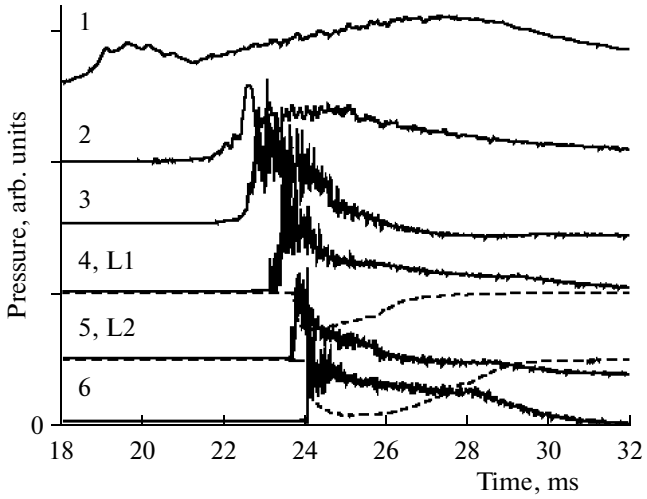

Fig. 5. Pressure profiles recorded by sensors 1–6 (solid curves) and luminescence intensity profiles recorded by photodiodes L1 and L2 (dashed curves) in experiment VI.

mixture was introduced in it. Another difference between the conditions of experiment V from those of experiments II and IV is the presence of a second perforated partition, designed for intensifying the combustion of the mixture.

Figure 4 shows pressure profiles (recorded by sensors 1–6) and luminescence emission profiles (recorded by photodiodes L1 and L2) in experiment V. It can be seen that, in this experiment, an intensive shock wave arises at the very beginning of the test section portion with turbulizing obstacles (sensor 3), and within this area (between sensors 3 and 4) its speed reaches ~1400 m/s. The time of arrival of the shock wave at sensor 4 (Fig. 4) almost coincides with the beginning of deflection of the signal from photodiode L1, located in the same section of the test section; i.e., the shock wave–reaction zone complex propagates here by the mechanism of detonation in rough tubes, involving local self-ignitions of the mixture as a result of multiple reflections of the shock wave from obstacles.

After the shock wave leaves the portion with turbulizing obstacles and enters the smooth portion of the test section, the speed of its propagation rapidly decreases to 850–900 m/s and then remains approximately constant. Such a decrease in the wave velocity is caused by a change in the conditions under which the chemical reactions behind the shock front occur: within the smooth portion of the test section, no local self-ignitions of the mixture at multiple reflections of the shock wave from obstacles occur. Interestingly, the time of arrival of the shock wave at sensor 5 (Fig. 4) also almost coincides with the deflection of the luminescence signal of photodiode L2, located at the same section in the smooth portion of the test section. In our opinion, the reason for which the shock wave–reaction zone complex continues to propagate by the mechanism of detonation in rough tubes is associated with a significant heterogeneity of the flow in the smooth tube after the shock wave leaves the portion of the tube obstructed with turbulizing obstacles. The rapid spontaneous self-ignition of the mixture behind the shock front at the wall of the tube could be caused by ongoing reflections of transverse shock waves, which inevitably make the wave front essentially non-one-dimensional.

Thus, the high-velocity shock wave–reaction zone complex can arise and propagate in a stoichiometric methane–air mixture even without activating the ignition with a small amount of methane–oxygen mixture. Such a complex in experiment V was produced only by increasing the rate of combustion of the mixture in the booster by placing an additional perforated partition.

In experiment VI (Table 1), a ring aperture was set between the booster and the test section to reduce the flow cross section by 67%, all other conditions being the same as in experiment V. The objective of experiment VI was to study the effect of the linear velocity of gas outflow from the booster (and hence the level of turbulization of the fresh mixture in the test section) on the dynamics of the formation of the shock wave–reaction zone high-velocity complex. The results of experiment VI are presented in Fig. 5. In contrast to experiment V, in experiment VI, a shock wave with a relatively gradual pressure rise enters the tube portion with turbulizing obstacles, not a shock wave with a sharp front (Fig. 4). Nevertheless, within the tube portion with turbulizing obstacles, this wave transforms into a shock wave and propagates at a velocity of ~1300 m/s. Interestingly, in contrast to experiment V, in experiment VI, the luminescence front (signal from photodiode L1 in Fig. 5) at the location of pressure sensor 4 lags behind the leading shock wave by ~500 μs. This means that, in the shock wave–reaction zone high-speed complex,

the mechanism of propagation of the reaction zone apparently changes: it propagates due to the rapid combustion of strongly turbulized volumes of fresh mixture near obstacles as they encounter the propagating turbulent flame. As in experiment V, in experiment VI, the velocity of the shock wave after it reaches the smooth portion of the test section decreased from ~1300 m/s to 850–900 m/s. In this case, the time lag of the reaction zone (signal from photodiode L2 in Fig. 5) behind the shock wave (pressure sensor signal in Fig. 5) remains at a level of 500 μs.

The results of experiment VI indicate that an increase of the flow velocity and turbulence intensity in the fresh mixture facilitates the establishment of hazardous modes of combustion of methane mixtures.

CONCLUSIONS

Thus, the experiments performed showed that the combined effect of acceleration of the flow due to the passage of the combustion wave from a larger-diameter tube (booster) into a smaller-diameter tube (test section) and through turbulizing obstacles significantly reduces the distance of the formation of the shock wave–reaction zone complex in a stoichiometric methane–air mixture: such a complex can be formed in a tube with turbulizing obstacles within a distance of ~1 m (~14 diameters of the test section) from the ignition source and can propagate in such a tube at a velocity of 1300–1400 m/s. After the passage of the shock wave–reaction zone complex from the tube portion with turbulizing obstacles into the smooth portion, it propagates there at a velocity of 850–900 m/s, without substantial attenuation, at least over a distance of 0.5–1 m.

Note that, in experiments with tubes of constant diameter 174 and 520 mm equipped with regular turbulizing obstacles [14], the shock wave velocity of 1300–1400 m/s was achieved within distances of 40 and 30 diameters, respectively, which is 2–3 times higher than in our experiments. Experiments [20] with the passage of normal gas detonation into a constant-diameter tube with Shchelkin spiral showed that, in such a tube, the shock wave–reaction zone complex propagates at a velocity not higher than 1000 m/s. All this suggests that transient combustion processes in ducts composed of commutating channels of different diameters and containing potions with turbulizing obstacles can be more dangerous and destructive than combustion in obstructed constant-diameter tubes.

ACKNOWLEDGMENTS

This work was supported by the Ministry of Education and Science of the Russian Federation under state contracts no. 16.526.12.6018 "Development of the High-Speed Energy-Saving Pulse-Detonation Gas Burner for Enhancement of the Performance of Furnaces and Power Installations."

REFERENCES

1. A. A. Borisov and S. A. Loban', Fiz. Goreniya Vzryva, No. 5, 729 (1977).
2. R. Knystautas, C. Guirao, J. H. Lee, and A. Sulmistras, Progr. Astronaut. Aeronaut. **94**, 23 (1984).
3. S. M. Frolov, V. S. Aksenov, and A. A. Skripnik, Dokl. Phys. Chem. **436**, 10 (2011).
4. P. Wolanski, C. W. Kauman, M. Sichel, and J. A. Nicholls, Proc. Combust. Inst. **18**, 1651 (1981).
5. S. M. Kogarko, Sov. Tech. Phys. **3**, 1904 (1958).
6. A. A. Borisov, in *Gaseous and Heterogeneous Detonations: Science to Applications*, Ed. by G. Roy, S. Frolov, K. Kailasanath, and N. Smirnov (ENAS Publ., Moscow, 1999), p. 3.
7. W. Bartknecht, *Explosion* (Springer, Berlin, 1981).
8. K. I. Shchelkin, *Fast Combustion and Spin Gas Detonation* (Voenizdat, Moscow, 1949) [in Russian].
9. R. P. Lindstedt and H. J. Michels, Combust. Flame **76**, 169 (1989).
10. H. Matsui, J. de Phys. IV **76**, Pr7 (2002).
11. A. A. Vasil'ev, in *Confined Detonations and Pulse Detonation Engines*, Ed. by G. Roy, S. Frolov, R. Santoro, and S. Tsyganov (Torus Press, Moscow, 2003), p. 41.
12. S. M. Frolov, V. S. Aksenov, V. S. Ivanov, S. N. Medvedev, V. A. Smetanyuk, K. A. Avdeev, and F. S. Frolov, Russ. J. Phys. Chem. B **5**, 625 (2011).
13. M. Kuznetsov, V. Alekseev, I. Matsukov, and T. H. Kim, in *Proceedings of the 8th ISHPMIE* (Jokohama, Japan, 2010), paper No. ISH-118.
14. M. Kuznetsov, G. Ciccarelli, S. Dorofeev, et al., Shock Waves **12**, 215 (2002).
15. S. M. Frolov, V. S. Aksenov, K. A. Avdeev, A. A. Borisov, P. A. Gusev, V. S. Ivanov, A. S. Koval, S. N. Medvedev, V. A. Smetanyuk, F. S. Frolov, and I. O. Shamshin, Dokl. Phys. Chem. **449**, 91 (2013).
16. S. M. Frolov, V. S. Aksenov, K. A. Avdeev, A. A. Borisov, V. S. Ivanov, A. S. Koval, S. N. Medvedev, V. A. Smetanyuk, F. S. Frolov, and I. O. Shamshin, Russ. J. Phys. Chem. B **7**, 137 (2013).
17. R. K. Zipf, V. N. Gamezo, M. J. Sapko, et al., J. Loss Prevent. Process Industries **26**, 295 (2013).
18. S. M. Frolov, Russ. J. Phys. Chem. B **2**, 442 (2008).
19. J. H. S. Lee, R. Knystautas, and A. Feiman, Combust. Flame **56**, 227 (1984).
20. Ya. B. Zeldovich, A. A. Borisov, B. E. Gelfand, S. V. Khomik, and A. E. Mailkov, Dokl. Akad. Nauk SSSR **279**, 1359 (1984).
21. Ya. B. Zeldovich, B. E. Gelfand, Ya. M. Kazhdan, and S. M. Frolov, Fiz. Goreniya Vzryva, No. 3, 103 (1986).
22. B. E. Gelfand, S. M. Frolov, and M. A. Nettleton, Progr. Energy Combust. Sci. **17** (4), 327 (1991).
23. S. M. Frolov, Tyazhel. Mashinostroen., No. 9, **18** (2003).
24. B. E. Gelfand, S. M. Frolov, and S. P. Medvedev, Fiz. Goreniya Vzryva **26** (3), 91 (1990).

Translated by V. Smirnov